2D Finite Element modelling of plane-wave diffusive time-harmonic electromagnetic fields using adaptive unstructured grids

Antje Franke, Ralph-Uwe Börner, and Klaus Spitzer,
Technische Universität Bergakademie Freiberg, Institute of Geophysics, Freiberg, Germany

Summary

We present a new adaptive unstructured triangular grid Finite Element approach for effectively simulating electromagnetic fields in two-dimensional anisotropic conductivity structures. This requires the elaborate generation of huge irregular grids and their expensive administration to model nearly arbitrary geometries including surface topography.

To characterise the diffusion of the electromagnetic fields, a second order elliptic boundary value problem is solved. The appropriate inhomogeneous Dirichlet boundary conditions are calculated analytically for a 1D stratified ground.

The accuracy of the Finite Element solution is mainly influenced by mesh parameters, in particular the size of the triangles. However, fine meshes and thus large grids require great effort in computing time and memory. Adaptively refined meshes generate fine discretisations only where necessary and therefore obtain optimum trade-off between computational expense and quality.

Comparisons to analytical solutions and numerical calculations illustrate the robustness and flexibility of our FE approach with respect to model geometry and topography.

1 Introduction

Numerical modelling in magnetotellurics (MT) has generally been carried out using regularly structured grids. Finite difference (FD) methods approximate solutions on rectangular grids that discretise regions into piecewise constant parameter structures (Jones and Price, 1970, Brewitt-Taylor and Weaver, 1976, Mackie et al., 1993). Finite element (FE) approaches are basically not restricted to such orthogonal model geometries. Using triangles in 2D and tetrahedrons in 3D, a much more flexible outlining of structural boundaries may be achieved by employing non-uniform grids. However, for the sake of simplicity, FE approaches were implemented on regularly structured grids by decomposing rectangles into triangles and prisms into tetrahedrons (Coggon, 1971, Wannamaker et al., 1987). Thus, the full power of such discretisation techniques has not unfolded so far.

We present a 2D FE algorithm for modelling electromagnetic fields using adaptive unstructured grids to discretise areas including anisotropic conductivities and surface topography. This approach benefits from all the advantages of the FE method. Meshes are refined by an *a-posteriori* error estimator only where necessary optimising run time and accuracy. Our results for anisotropic models are compared to those obtained from an FE code by Li (2000) and an FD code by Pek and Verner (1997).

2 The Boundary Value Problem

The behaviour of plane-wave time-harmonic diffusive electromagnetic fields is governed by Maxwell's equations in the quasi-static approximation. They lead to a second-order elliptic partial differential equation (pde) of the general form

$$-\nabla \cdot (c \cdot \nabla u) + a \cdot u = f. \tag{1}$$

Let y be the strike direction of a 2D conductivity structure and $\sigma = \sigma(x,z)$ be the isotropic conductivity. The coordinate system is right-handed with the z-axis pointing negative downwards. In case of dipping anisotropy the conductivity tensor is

$$\tilde{\sigma} = \begin{pmatrix} \sigma_{xx} & 0 & \sigma_{xz} \\ 0 & \sigma_{yy} & 0 \\ \sigma_{zx} & 0 & \sigma_{zz} \end{pmatrix}. \tag{2}$$

For E-Polarisation we have $\vec{E} = (0, E_y, 0)^T$ and for H-Polarisation $\vec{H} = (0, H_y, 0)^T$. The following definitions are valid for the coefficients a, c, and the right hand side f of eq. (1):

- E-polarisation: $u := E_y$

$$\begin{aligned} \text{isotropic:} \quad & c := 1, \\ & a := i\omega\mu\sigma, \\ & f := 0, \\ \text{anisotropic:} \quad & c := 1, \\ & a := i\omega\mu\sigma_{yy}, \\ & f := 0, \end{aligned} \tag{3}$$

- H-polarisation: $u := H_y$

$$\begin{aligned} \text{isotropic:} \quad & c := 1/\sigma, \\ & a := i\omega\mu, \\ & f := 0, \\ \text{anisotropic:} \quad & c := 1/\tau \begin{pmatrix} \sigma_{xx} & \sigma_{xz} \\ \sigma_{zx} & \sigma_{zz} \end{pmatrix}, \\ & \tau = \sigma_{xz}\sigma_{zx} - \sigma_{xx}\sigma_{zz}, \\ & a := i\omega\mu, \\ & f := 0. \end{aligned} \tag{4}$$

$\mu = \mu_0 = 4\pi \cdot 10^{-7}\, Vs \cdot (Am)^{-1}$ is the free space magnetic permeability and ω the angular frequency of the observed time-harmonic fields.

To solve for the unknown field components, appropriate boundary conditions need to be introduced. At the vertical outer domain boundaries, the analytical solution for a layered halfspace is given (Wait, 1953). Li (2000) presents a straightforward calculation of boundary conditions for arbitrarily anisotropic conductivity structures. The field values at the horizontal upper and lower boundaries are obtained by a cubic spline interpolation.

3 The Finite Element Method

In the FE method, a piecewise linear approximation u_h to the exact solution u is sought in the closed region $\bar{\Omega} = \Omega \cup \Gamma$ with the inner part Ω and the outer boundaries Γ. Therefore we test the elliptic pde $Lu_h = f$ against all possible test functions v of that class:

$$\int_{\bar{\Omega}} (Lu_h - f)v \, dx = 0. \tag{5}$$

L is an elliptical differential operator (cf. eq. (1)). u_h is represented as a combination $u_h(x) = \sum_{i=1}^{n} U_i N_i(x)$ with piecewise linear basis functions N_i (Fig. 1) and scalar coefficients U_i. To determine n unknowns $U_1, U_2, ..., U_n$ we choose n test functions to be $v = N_1, N_2, ..., N_n$. This results in a system of linear equations

$$(\tilde{K} + \tilde{M})\, \vec{u} = 0, \tag{6}$$

where the stiffness matrix $\tilde{K}$ and the mass matrix $\tilde{M}$ contain integrals in terms of the basis functions N_i^e, N_j^e on triangle e, as well as the coefficients a and c defining the problem

$$\begin{aligned} \tilde{K}^e &= \iint_{\Omega^e} \Big((c \cdot \nabla\, N_j^e) \cdot \nabla\, N_i^e \Big) dxdy, \\ \tilde{M}^e &= \iint_{\Omega^e} a N_i^e N_j^e dxdy \end{aligned} \tag{7}$$

for a single element e with area Ω_e. The vector $\vec{u}$ contains the field values $H_{y,i}$ or $E_{y,i}$ at each mesh point i. Considering the correlation between the local and global numbering of the grid nodes the element matrices $\tilde{K}^e$ and $\tilde{M}^e$ are assembled to constitute $\tilde{K}$ and $\tilde{M}$, respectively.

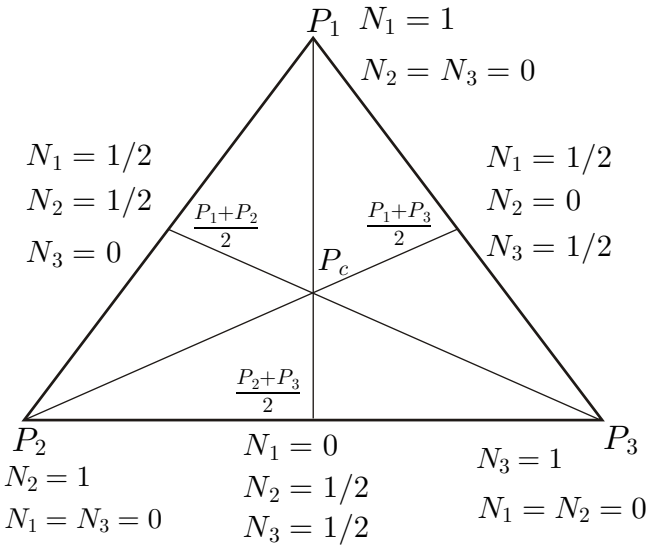

Fig. 1: Linear basis functions $N_i^e(P_j)$ $(i,j = 1,2,3)$ on triangle e, $N_i^e(P_j) = 1$ $(i = j)$ and $N_i^e(P_j) = 0$ $(i \neq j)$.

The solution $\vec{u} = \vec{u}_\Omega + \vec{u}_\Gamma$ is composed of field values $\vec{u}_\Omega$ at the inner points in region Ω and $\vec{u}_\Gamma$ on the boundaries Γ. The Dirichlet boundary conditions $\vec{u}_\Gamma = \vec{E}, \vec{H}$ are considered separately. From eq. (6) we derive a system of linear equations for $\vec{u}_\Omega$:

$$(\tilde{K} + \tilde{M})\, \vec{u}_\Omega = -(\tilde{K} + \tilde{M})\, \vec{u}_\Gamma. \tag{8}$$

The quality of an FE solution can be remarkably improved by reducing the size of the grid elements. Unlike refining a mesh globally, an adaptive refinement strategy yields an optimal mesh with even less triangles (Fig. 2). The regions for adaptive mesh refinement are determined on the basis of an *a-posteriori* error estimator that considers the residual $f - au_h$ of eq. (1) on each triangle and the jump in flux $\vec{n} \cdot c\nabla u_h$ across the element edge. For linear basis functions we have $\nabla \cdot c\nabla u_h = 0$. $\vec{n}$ is the unit normal vector of the appropriate edge. A direct solver of the Gauß elimination type is applied to eq. (8). Jin (1993) and Monk (2003) are recommended for further reading about FE applications in electromagnetics. Due to the complexity of an FE implementation using unstructured grids we have utilised the MATLAB®pde toolbox for solving partial differential equations.

4 Comparison with Analytical Solutions

We have carried out simulations for different homogeneous halfspaces at a fixed frequency and for a layered halfspace using a set of frequencies. The results indicate that the accuracy of the calculated fields for a given grid is mainly dependent on the skin depth. Even for an adaptively refined mesh the number of grid nodes per skin depth is limited by the total addressable memory space (here around 300,000 triangles at 1 GB RAM).

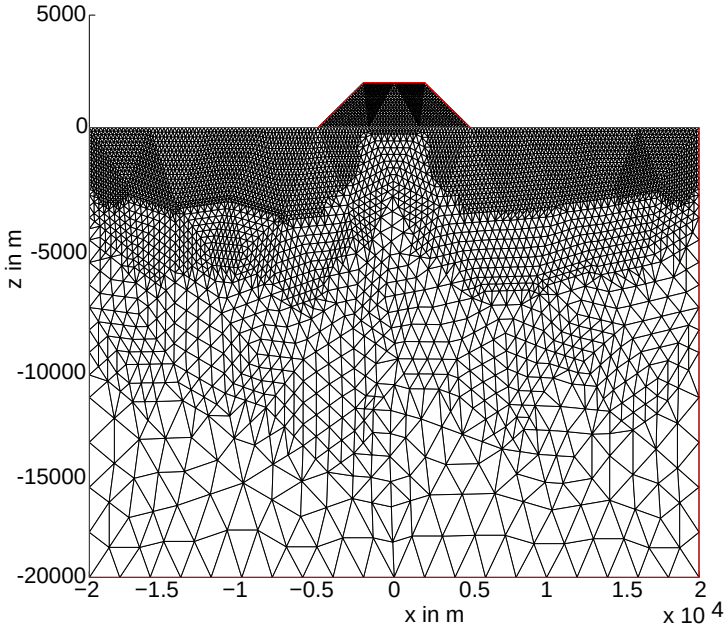

Fig. 2: Adaptively refined mesh for an H-Polarisation model with surface topography.

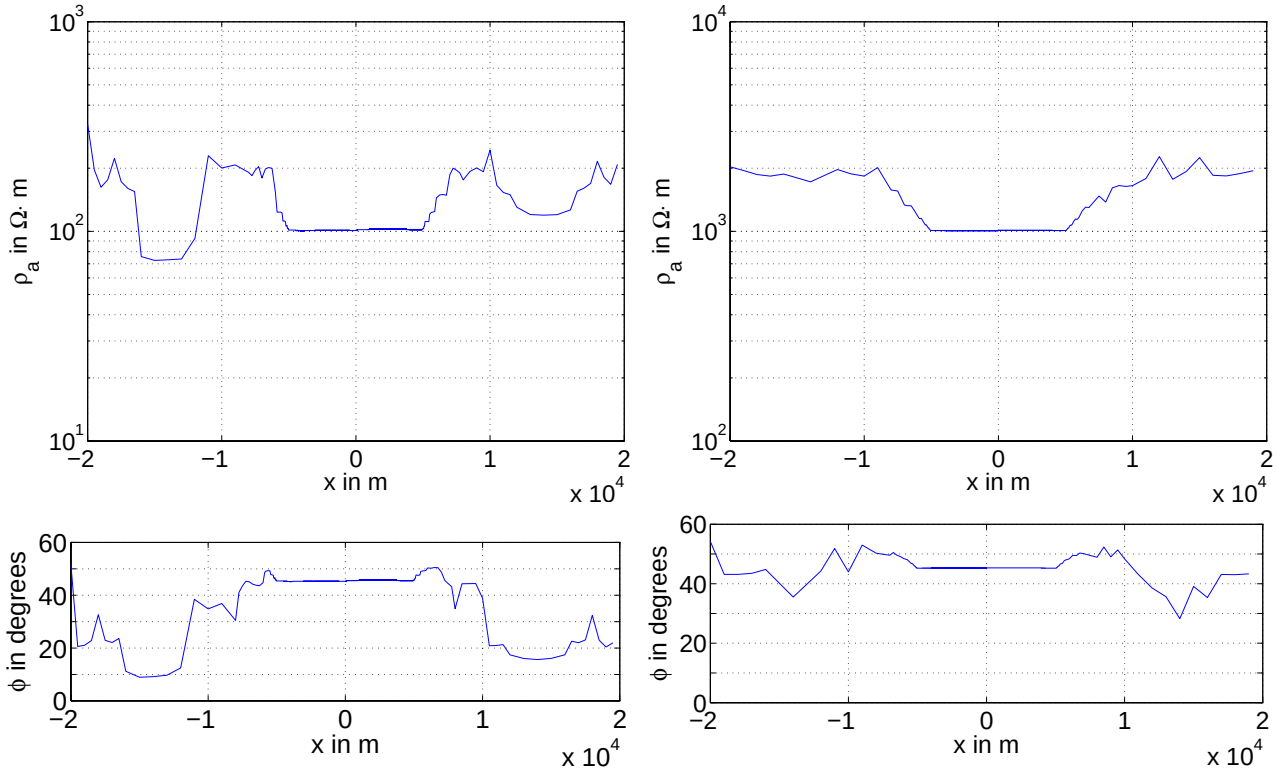

Fig. 3: Apparent resistivity ρ_a (top) and phase angle ϕ (bottom) at the surface of a $100\,\Omega$m (left) and a $1000\,\Omega$m (right) halfspace at a frequency of $f = 1\,$kHz, E-Polarisation, adaptive mesh refinement for $-5000\,\text{m} \leq x \leq 5000\,\text{m}$, error in adaptive refined region: $\delta_{\rho_a} \leq 2.5\%$, $\delta_\phi \approx 0.7$ degrees (left), $\delta_{\rho_a} \leq 1.5\%$, $\delta_\phi \approx 0.5$ degrees (right).

In Fig. 3, the 1000 Ωm halfspace solution (right) shows higher accuracy in apparent resistivity (top) and phase angle (bottom) than that of the 100 Ωm halfspace (left). Note, that the region of adaptive mesh refinement extends from $x = -5000$ m to $x = 5000$ m. The electromagnetic soundings in Fig. 4 are simulated for a 100 Ωm halfspace containing a layer of 10 Ωm between $z = -200$ m and $z = -300$ m. Again, the discrepancies at low periods are due to the appropriate small skin depths being covered by only few grid nodes. The accuracy may be enhanced further by adapting the model size to the frequency range.

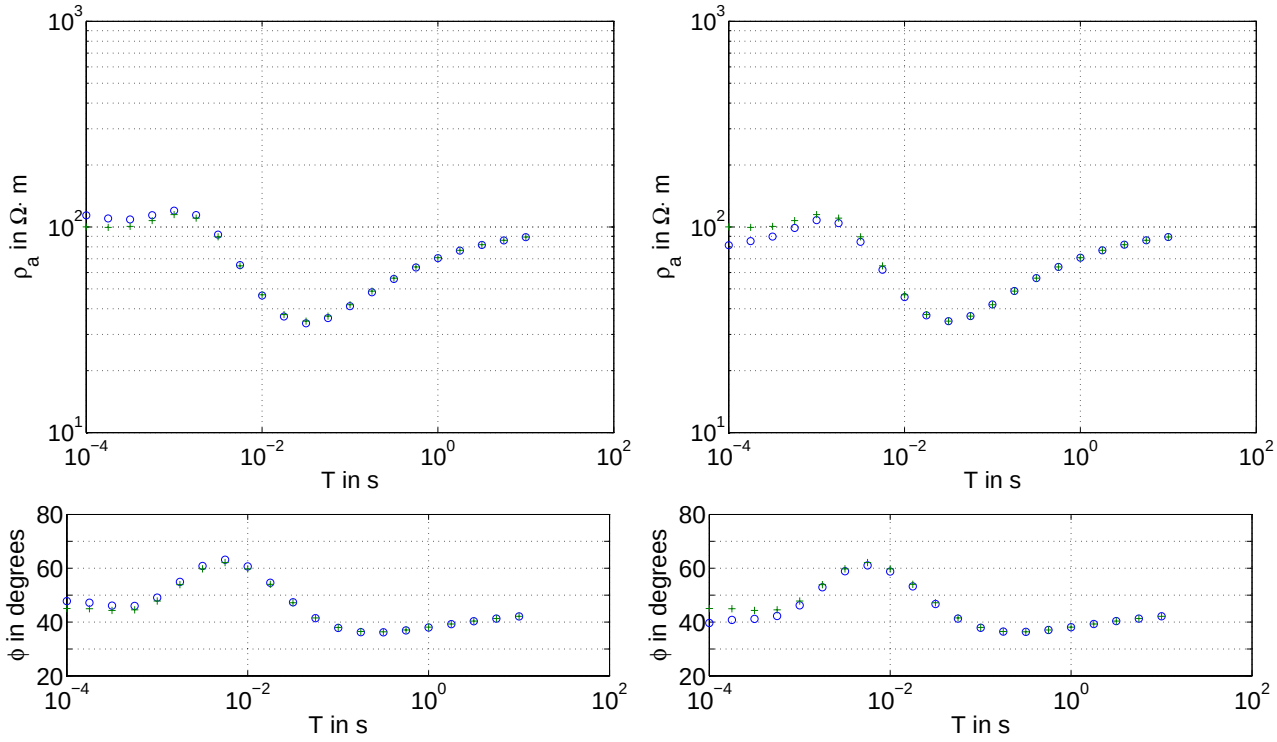

Fig. 4: Soundings of apparent resistivity ρ_a (top) and phase angle ϕ (bottom) over a 100 Ωm halfspace with an embedded 10 Ωm layer between −200 m and −300 m depth, analytic '+' (green) and numeric 'o' (blue) solution, E- (left) and H- (right) Polarisation, max. error: $\delta_{\rho_a} \leq 14\%$, $\delta_\phi \approx 2.8$ degrees (left), $\delta_{\rho_a} \leq 15\%$, $\delta_\phi \approx 5.4$ degrees (right).

5 Comparison with Numerical Calculations

One of the 2D COMMEMI (Comparison of modeling for Methods of Electromagnetic Induction) models was used as an example for comparing our FE approach with an FE program by Li (2000) and with an FD code by Weaver (1986).

Fig. 5 displays the COMMEMI model 2D-4. The apparent resistivity computed by our algorithm and the two reference codes for this model is shown in Fig. 6 for E- and H-Polarisation on the left- and right-hand side, respectively. The results are in good agreement.

Figs 7 and 8 present the horizontal current densities j_y and j_x for E- and H-Polarisation. In both cases, the currents are focussed in the upper conductive zones and decay with depth. Some channeling occurs in the thin 2.5 Ωm layer. j_y (Fig. 7) is discontinuous at horizontal conductivity contrasts whereas j_x (Fig 8) is continuous. In the right-hand diagrams large values of the imaginary parts of the current density $Im(j_y)$ (Fig. 7) and $Im(j_x)$ (Fig. 8) reflect strong induction effects in the conductive layers.

6 Anisotropy

Our FE approach is compared to the FD algorithm by Pek and Verner (1997) on the basis of the anisotropic dike model depicted in Fig. 9.

Fig. 10 displays the results computed by our FE approach and the FD reference algorithm in terms of apparent resistivity (top) and phase angle (bottom) for E- (right) and H- (left) Polarisation, respectively.

The dike structure leads to decreased apparent resistivity in both polarisation modes because all components of the dike's conductivity tensor are larger than the halfspace conductivity. However, the phase shows opposite behaviour for E- and H-Polarisation. This is due to the different directions of the currents. The asymmetry displayed in all curves is caused by the anisotropy.

Our results agree well with the values derived from the FD code. Higher deviations only occur within the dike and on its edges. At the conductivity contrasts the conditions of continuity are required for the electromagnetic field components. In the FE case, the mesh is generated adaptively on the basis of an error estimator. The FD grid is set up manually. It is coarser in the region of the conductivity contrast so that we assume our result to be more accurate.

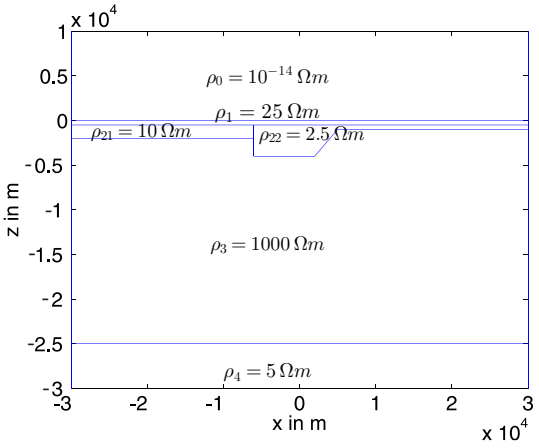

Fig. 5: COMMEMI model 2D-4.

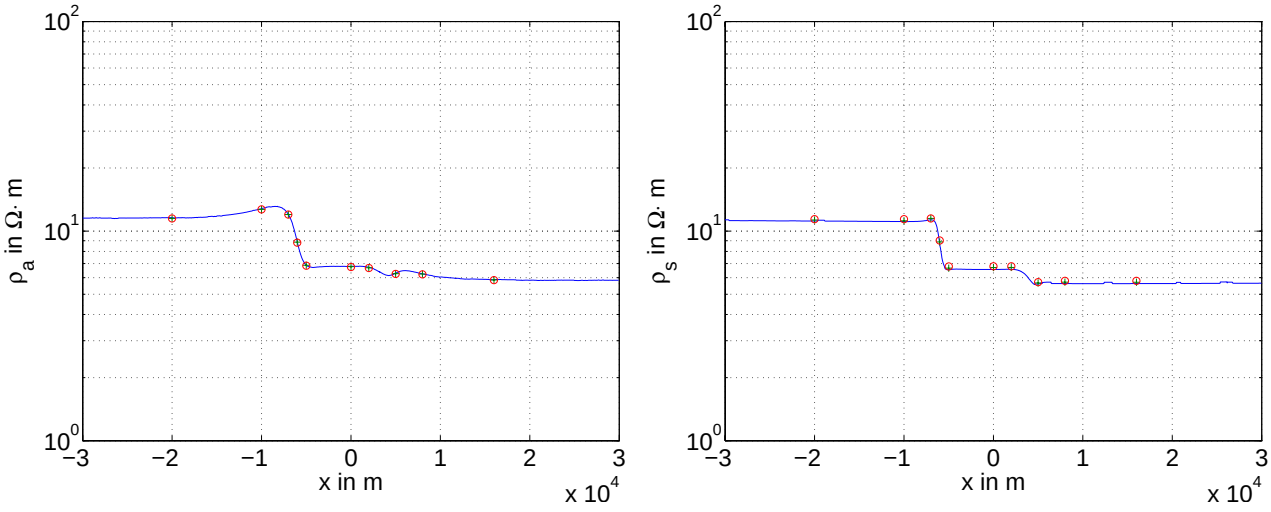

Fig. 6: Apparent resistivitiy ρ_a computed with our FE code '–', the one by Li '+', and the one by Weaver 'o' for E- (left) and H- (right) Polarisation. Deviations are about 2%.

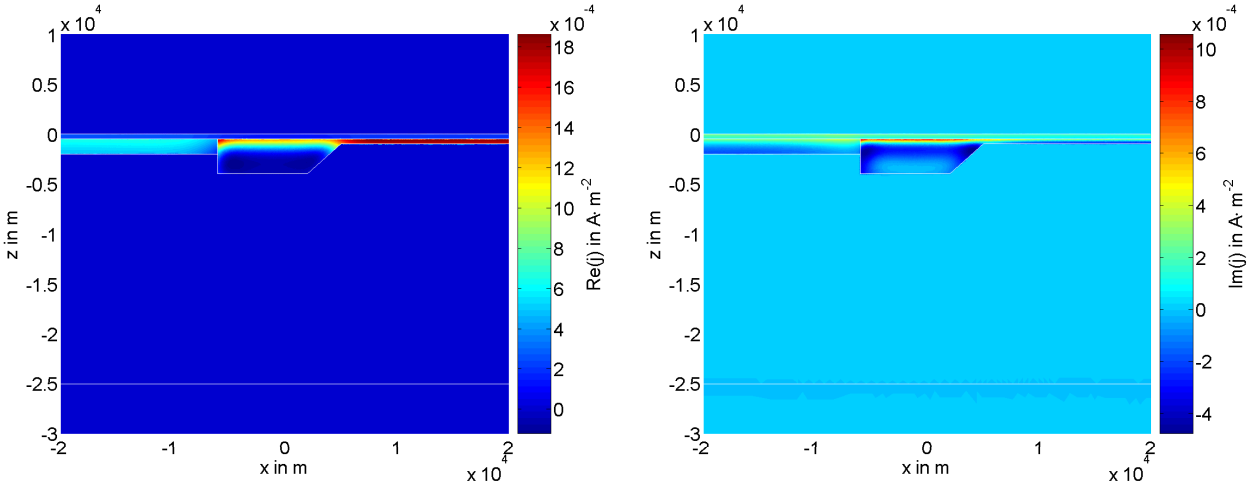

Fig. 7: Real (left) and imaginary (right) part of current density j_y, E-Polarisation.

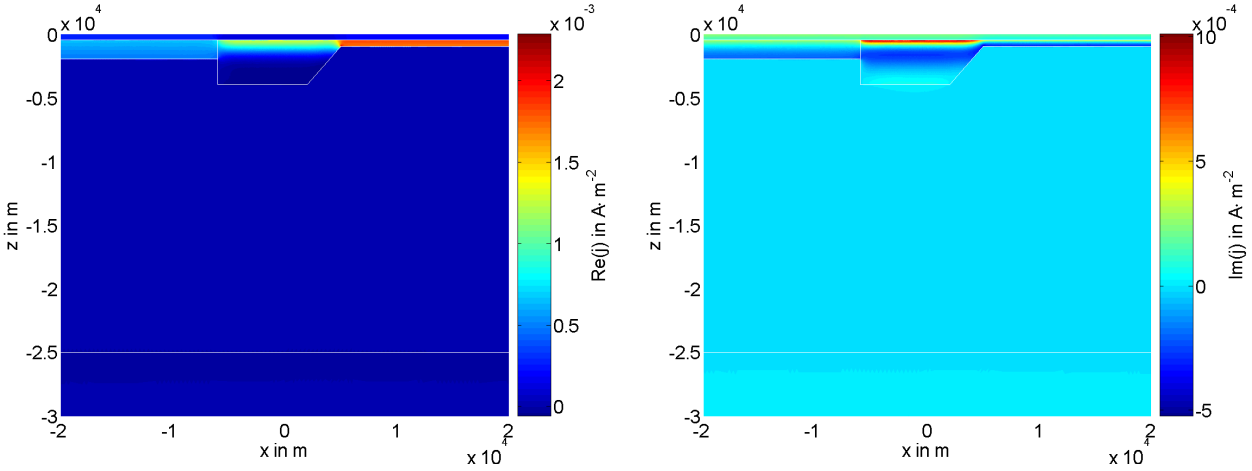

Fig. 8: Real (left) and imaginary (right) part of the current density j_x, H-Polarisation.

7 Topography

Wannamaker et al. (1986) discussed the topographic responses of simple-structured earth's surfaces. They applied triangular FE meshes that result from the decomposition of rectangular grid cells. However, unstructured grids provide the more precise discretisation of arbitrary model geometries. Exemplary, the topographic effects of a sinusoidal ($z = -\Delta cos(\frac{2\pi}{\lambda}x)$, $\Delta = 100\,m$ and $\lambda = 1000\,m$) land surface are examined.

Fig. 11 shows the real part of the current density components j_y and j_x for E- and H-Polarisation, respectively. In the case of j_y (left diagram) large current densities occur in the conductive earth especially on top of the hills. The lateral lack of current flow in the air results in a higher apparent resistivity and larger phases over the hills while the extra current flow near the valleys yields negative anomalies in apparent resistivity and phase angle (Fig. 12 left). On the contrary, in the case of H-polarisation the current density j_x (Fig. 11 right-hand side) displays high values in the valleys. This leads to a decreased apparent resistivity on top of the hills. However, the phase depends on the direction of the currents as well so that it shows the same general tendency as for E-Polarisation.

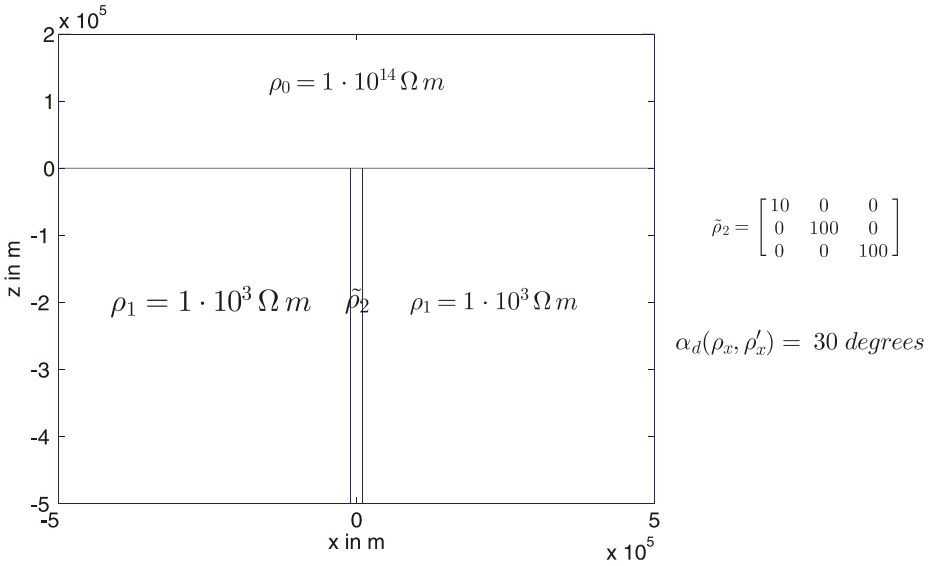

Fig. 9: Model of an anisotropic dike located in an isotropic homogeneous halfspace.

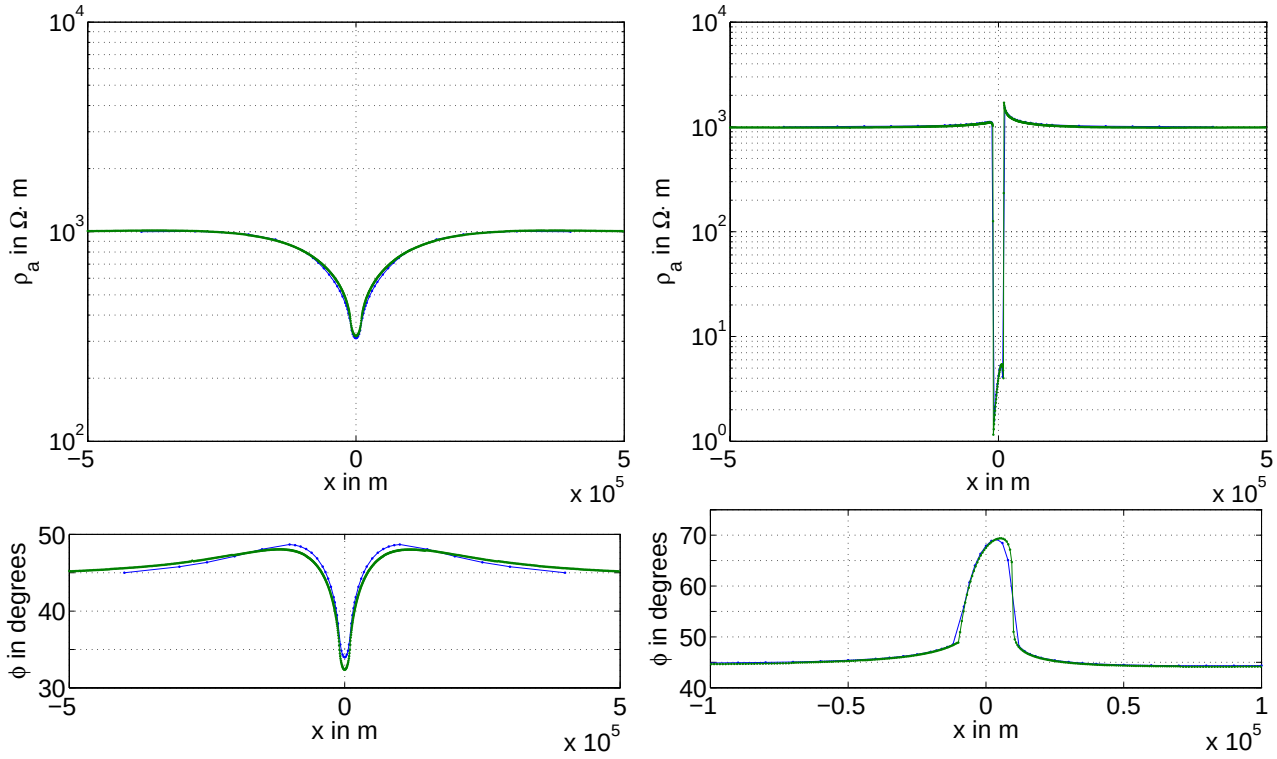

Fig. 10: Apparent resistivity ρ_a (top) and phase angle (bottom) ϕ for the dike model (Fig. 9) computed by the FE (green) and the FD (blue) code at a frequency of $f = 0.01$ Hz, E- (left) and H-Polarisation (right), deviations: $\Delta\rho_a \leq 6\%$, $\Delta\phi < 1.6$ degrees, within the dike: $\Delta\rho_a \leq 20\%$, $\Delta\phi \leq 3.2$ degrees.

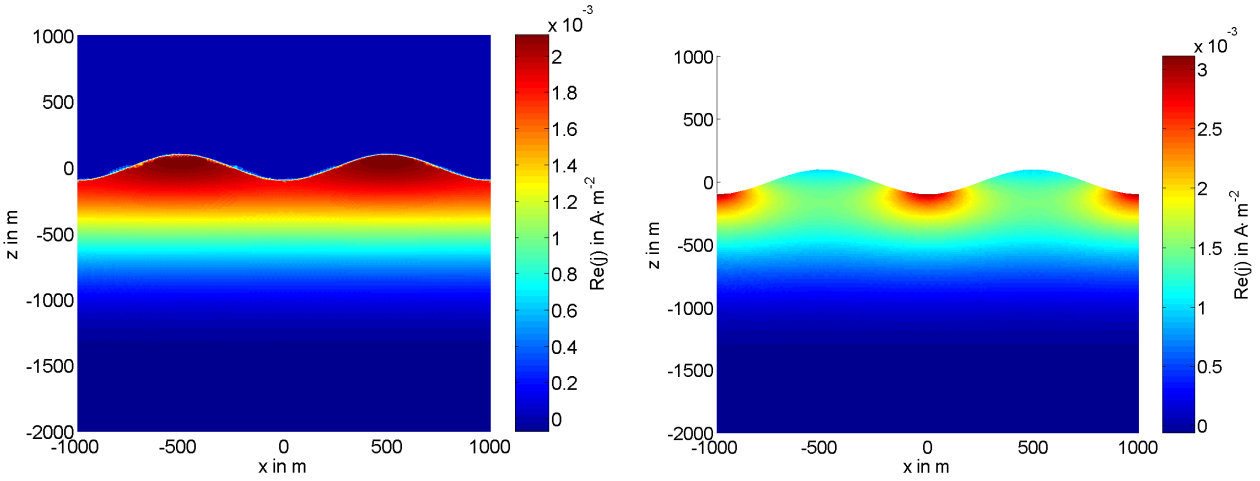

Fig. 11: Real part of current density $Re(j_y)$, E-Polarisation (left) and real part of current density $Re(j_x)$, H-Polarisation (right), $\rho_0 = 10^{14}\,\Omega m$ (air), $\rho_1 = 100\,\Omega m$ (crust), $f = 100\,Hz$.

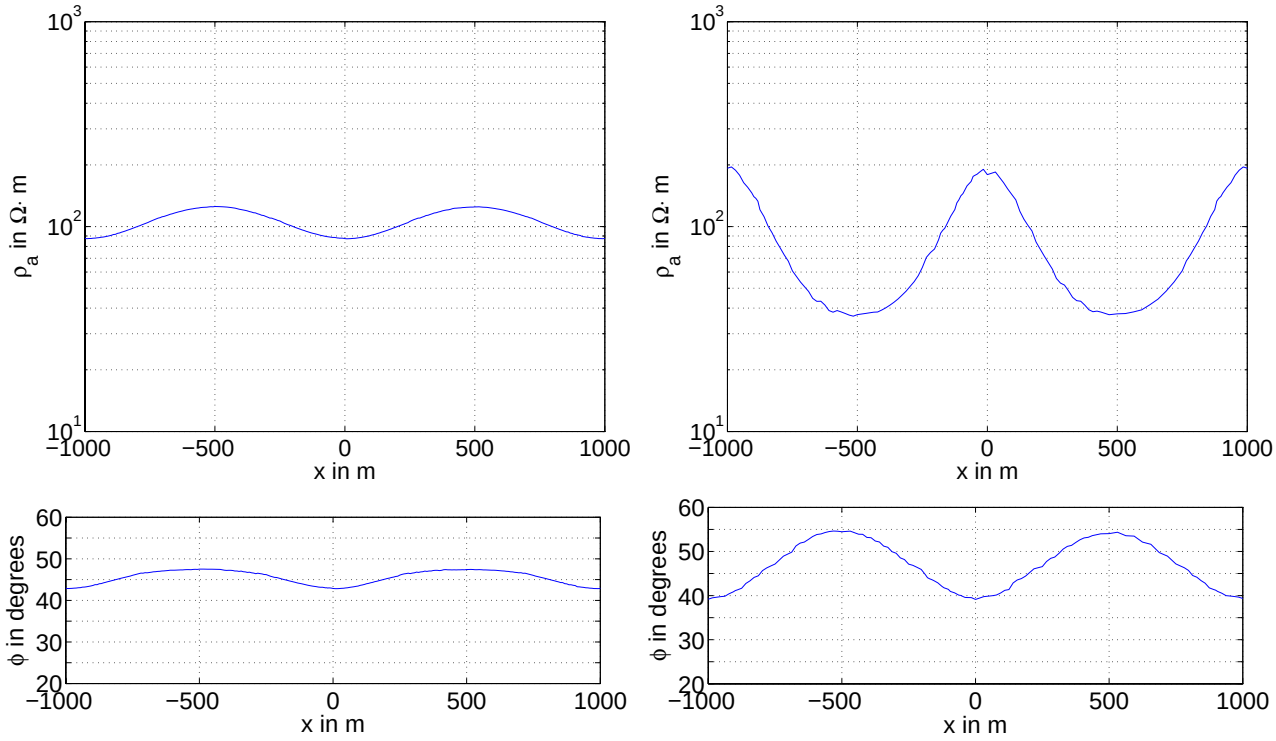

Fig. 12: Apparent resistivity ρ_a (top) and phase angle ϕ (bottom), E- (left) and H- (right) Polarisation.

8 Conclusions

We have developed an FE approach for modelling plane-wave diffusive electromagnetic fields. The appropriate boundary value problem consists of an elliptic second-order partial differential equation including inhomogeneous Dirichlet boundary conditions. A system of linear equations results from applying the FE approximation with linear basis functions on unstructured triangular grids. So far, direct equation solvers are sufficient to obtain the solutions in reasonable times.

A comparison with analytical solutions and numerical calculations has shown that our FE approach is numerically robust. The use of unstructured grids is very suitable for simulating electromagnetic fields in arbitrary model geometries especially if surface topography is involved. This seems to be very promising with regard to bathymetric data in marine geophysics.

Adaptive mesh generation guarentees high accuracy allowing for the efficient utilisation of computer memory.

The good experience with a commercial software toolbox encourages us to continue our strategy of integrating existing software for purely admininstrative software engineering reasons. This means cautious and controlled outsourcing of code generation with the aim of decreased development times, however, without loss of transparency.

Acknowledgements

Thanks to Y. Li for useful hints on boundary conditions for arbitrarily anisotropic conductivity structures and providing the results of his as well as J.T. Weaver's reference codes. The authors are grateful to J. Pek for making his FD algorithm available.

References

Brewitt-Taylor, C. and Weaver, J. (1976). On the finite difference solution of two-dimensional induction problems. *Geophys. J. R. astr. Soc.*, *47*, 375-396.

Coggon, J. H. (1971). Electromagnetic and electrical modeling by the finite element method. *Geophysics*, *36*, 132-155.

Jin, J. (1993). *The finite element method in electromagnetics*. John Wiley & Sons, Inc.

Jones, F. W. and Price, A. T. (1970). The perturbations of alternating geomagnetic fields by conductivity anomalies. *Geophys. J. R.l astr. Soc.*, *20*, 317-334.

Li, Y. (2000). *Numerische Modellierungen von elektromagnetischen Feldern in 2- und 3-dimensionalen anisotropen Leitfähigkeitsstrukturen der Erde nach der Methode der Finiten Elemente*. PhD thesis, Universität Göttingen, Cuvillier Verlag Göttingen.

Mackie, R. et al. (1993). Three-dimensional magnetotelluric modeling using difference equations - theory and comparisons to integral equation solutions. *Geophysics*, *58*, 215-226.

Monk, P. (2003). *Finite element methods for maxwell's equations*. Oxford University Press Inc., New York.

Pek, J. and Verner, T. (1997). Finite-difference modelling of electromagnetic fields in two-dimensional anisotropic media. *Geophysical Journal International*, *128*, 505-521.

Wait, J. R. (1953). Propagation of radio waves over a stratified ground. *Geophysics*, *20*, 416-422.

Wannamaker, P. E. et al. (1986). Two-dimensional topographic responses in magnetotellurics modeled using finite elements. *Geophysics*, *51*, 2131-2144.

Wannamaker, P. E. et al. (1987). A stable finite element solution for two-dimensional magnetotelluric modelling. *Geophys. J. R. astr. Soc.*, *88*, 277-296.

Weaver, J. T. (1986). *Finite difference calculations for commemi.* Department of Physics, University Victoria.

Weaver, J. T. (1994). *Mathematical methods for geo-electromagnetic induction*. Research Studies Press Ltd., John Wiley & Sons Inc.